Journal of Sound and Vibration (1985) **101**(2), 203-218

THE USE OF THE SONOGRAM IN STRUCTURAL ACOUSTICS AND AN APPLICATION TO THE VIBRATIONS OF CYLINDRICAL SHELLS

C. H. HODGES, J. POWER AND J. WOODHOUSE

Topexpress Limited, 13/14 Round Church Street, Cambridge CB5 8AD, England

(*Received* 24 *May* 1984, *and in revised form* 10 *September* 1984)

The time-varying spectrum, or sonogram, is a familiar tool in areas of acoustics concerned with perception—especially in speech studies. It can also be of great benefit in studies of wave propagation in structures, a fact which is less well known. Processing the impulse response of a structure at a distance from the driving point gives a direct measure of the group velocity as a function of frequency, a quantity not easy to measure by more conventional methods. The approach is illustrated by using simulated data from idealized models of a stretched string and a bending beam. These tests show how the features in the sonogram pictures vary with changes in the compromise between time resolution and frequency resolution: one can obtain a continuous change from a time-domain viewpoint to a frequency-domain one, learning on the way things not easily found from either extreme. The technique is applied to measurements of the different waveguide modes of a cylindrical shell, where it gives a rather stringent check against certain aspects of theory.

1. INTRODUCTION: APPLICATION TO THE STRETCHED STRING

In this paper, we investigate the use of a familiar tool in an unfamilar context. The time-varying spectrum, or sonogram, has been used widely in many areas of acoustics, especially in speech studies. However, it has not been used in any systematic way in studies of structural vibration. We shall try to encourage such use by showing how powerful it can be in these problems. We consider two idealized structures and show that the sonogram reveals certain features of their behaviour very clearly (particularly the group velocity as a function of frequency). We then apply the technique to some real data measured on a cylindrical shell, where it gives some useful insights not readily gained by other methods.

Consider first the behaviour of a stretched string. If a force impulse is applied at a point on the string, two equal velocity impulses will travel out in opposite directions at the wave speed of the string. They will reflect from the terminations of the string, and continue reflecting back and forth until dissipation makes them die away. The chain of events may be represented conveniently in a space-time diagram such as Figure 1(a). Time is plotted along the x-axis, and position of the impulses on the string along the y-axis. The two zig-zag lines represent the paths in space-time of the two velocity impulses started by the original force at the point marked A.

The dashed line represents the position of an observer. He will in general see four impulses within each round-trip period of the string: in other words a velocity waveform like that of Figure 1(b), which has the same timescale as Figure 1(a). Within each period the arrival times of the four impulses depend both on the position of the driving point and the position of the observing point, as is clear from the figure. The particular case

0020-460X/85/140203+16 $03.00/0

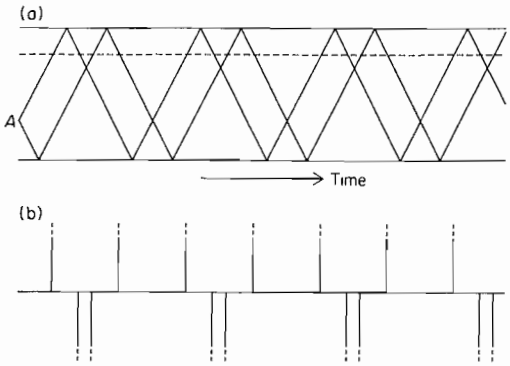

Figure 1. (a) Space-time diagram of impulses travelling on a stretched string; (b) time series seen by the observer represented by the dashed line in (a).

illustrated has the driving point and observing point at 3/10 and 4/5 of the total string length respectively.

The first way in which the observer might choose to analyze the time series of Figure 1(b) is as a power spectrum (autospectrum). The result, for the particular positions of driving and observing point shown in Figure 1, is illustrated in Figure 2. Precise details

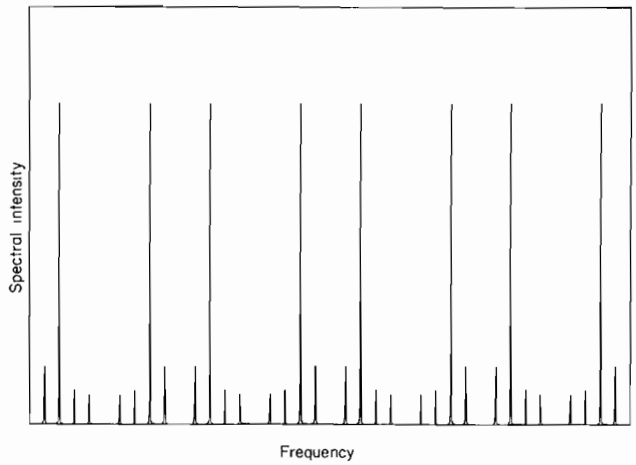

Figure 2. Power spectrum of the time series shown in Figure 1(b). Both scales are linear.

of how Figure 2 was calculated, along with all other such technical details, are given in the Appendix. One can see quite clearly discrete peaks corresponding to the vibration modes of the string, which are of course equally spaced in frequency. The heights of the peaks are modulated in a fairly complicated way, which reflects the positions of the driving and observing points. Basically, if the driving or observing point is one quarter of the way along the string, every fourth harmonic will be missing. Similarly, every fifth will be missing if either point is one-fifth of the way along the string, and so on.

Suppose now that the observer chooses to process the time series of Figure 1(b) as a time-varying spectrum, or sonogram. This is readily done once the time series has been digitized into a computer. He simply takes a portion of the time series, and Fourier

analyzes it. He ther
and so on. He wou
amplitude against
surface picture. (T
band, in which the
with power-spectra

There is a techni
above that a portio
one necessarily tak
Fourier transform
analysis, one may
side-lobes and the
the Hanning windo
any anomalous eff
put spurious, eye-c
to be much more s
because of these un
is not appropriate i
the Hanning windo

What such a son
"window" over whi
one can control the
there must be a trac
aspects of the sam
Uncertainty Princip
the window length
to a "travelling wa
other structure we a
length was not avai
of fixed bandwidth
there is a natural ter
tics of the human e

A sequence of so
Figures 3(a)-(d). A
The time range is s
frequency range is t
that plotting the res
on. The vertical axi
in Figure 2.

When the time w
Figure 3(a), one see
up the sonogram is
clearly seeing a "mo
the front edge of th
case makes the sign

When the windov
begins to see modu
frequency resolutio
variations in freque
individual peaks. A

analyzes it. He then takes another portion slightly later in time, and analyzes that similarly, and so on. He would then plot the result as a two-dimensional picture of power-spectral amplitude against time and frequency—this might be plotted as a contour map, or as a surface picture. (The original analogue machines produce a stripe for each frequency band, in which the width of the stripe and hence the blackness of the picture is modulated with power-spectral amplitude, giving the familiar "visible speech" pictures.)

There is a technical detail which warrants comment at this point. When it was stated above that a portion of the time series was to be Fourier analyzed, this is not to say that one necessarily takes a "rectangular window" of the time series and calculates the discrete Fourier transform of that. As with other calculations which call for digital frequency analysis, one may find it convenient to use other data windows in order to control side-lobes and the like. In the particular case of calculating sonograms, it is found that the Hanning window is a very good choice since it provides a very simple way of removing any anomalous effects of discontinuities in the signal at the window edges, which can put spurious, eye-catching features into the sonogram pictures. In fact, windowing proves to be much more significant in calculating sonograms than in ordinary spectral analysis because of these unwanted temporal features: however, a detailed discussion of this issue is not appropriate in this short paper. All the sonograms shown here were calculated with the Hanning window.

What such a sonogram reveals about the time series depends on the length of the time "window" over which the frequency analysis is performed. By varying this window length, one can control the trade-off between time resolution and frequency resolution: obviously there must be a trade-off, since time and frequency are not independent variables but are aspects of the same thing. Sonograms are subject to what is essentially Heisenberg's Uncertainty Principle. It turns out that the change in the sonogram pictures as one varies the window length mirrors the transition from a "mode viewpoint" (with a long window) to a "travelling wave viewpoint" (with a short window) of how the string (or whatever other structure we are considering) behaves. Note that the freedom to choose the window length was not available in the old analogue sonogram machines, since they had filters of fixed bandwidth. In any case, for measurements related to the perception of sound there is a natural temporal resolution, of the order of 70 ms or so, given by the characteristics of the human ear.

A sequence of sonograms corresponding to the time series of Figure 1(b) is shown in Figures 3(a)-(d). All four sonograms show the same range of both time and frequency. The time range is such as to contain three complete cycles of the time series, and the frequency range is the same as in Figure 2. For these particular sonograms, it was found that plotting the results as a view of a surface gives the clearest picture of what is going on. The vertical axis shows power-spectral amplitude, on a linear scale as was the case in Figure 2.

When the time window is long compared with the natural period of the string, as in Figure 3(a), one sees virtually no variation in time, since each individual spectrum making up the sonogram is more or less the same as the power spectrum of Figure 2. One is still clearly seeing a "modes" picture. The only time variation seen is a starting transient, since the front edge of the figure corresponds to time zero and the very long window in this case makes the signal appear to start slowly.

When the window length becomes comparable with the period, as in Figure 3(b), one begins to see modulation of the spectrum in time, and one pays for this by losing the frequency resolution which shows the individual mode peaks. One still sees strong variations in frequency, however, reflecting now the spectral envelope rather than the individual peaks. Another view of what is happening is that one has broadened the

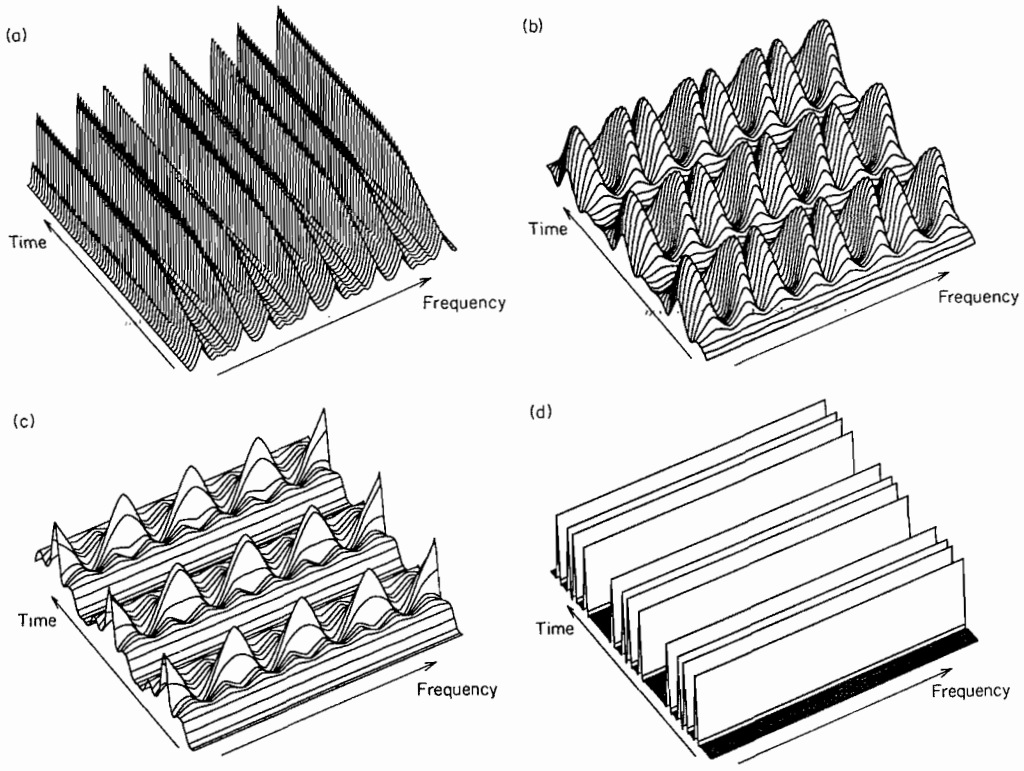

Figure 3. (a)–(d) Sonograms of the time series shown in Figure 1(b) with window lengths decreasing progressively from (a) to (d) as given in the Appendix.

frequency resolution so as to "smudge out" adjacent harmonics in the power spectrum, and the effect of this is to produce beating in time between these adjacent harmonics.

Making the window shorter still as in Figure 3(c), one has even less resolution in frequency but more resolution in time. What one has in this case is a window sufficiently short to resolve the first and the fourth impulses of each group of four (see Figure 1), but not short enough to resolve the middle pair, which are closer together in time. Thus for each cycle the figure shows first a ridge with no variation in frequency, then a higher ridge sinusoidally modulated in frequency coming from the interference of the second and third impulses, then another flat ridge corresponding to the fourth impulse. There is then a quiet spell, and the cycle repeats.

By the time the window is shorter than the separation of the second and third impulses, as in Figure 3(d), one is left with absolutely no frequency resolution, but one can now see the four separate impulses arriving at the observing point within each cycle, each impulse producing a flat ridge of the same height: we have reached a "travelling wave" picture which mirrors the original time series exactly.

An important point to note about the sequence of sonograms shown above is that although they look very different, they all contain essentially the same information. (Phase information is of course lost in any amplitude-only spectral analysis, but the main point being made here is that signal processing of any type does not create information.) Different forms of presentation of that information may have advantages in bringing out different features of the behaviour of the string, but one has not added any new information in going from one case to the next. Thus there is no "best" compromise on resolution in

an *a priori* sens
the best view o
convenient to p
sequence above
interesting and

It has now
thoroughly in a
technique to sti
applied to the i
simplicity of the
However, it doe
a beam with dif
the problem les

Figure 4. Time serie

This remark is
analogous to Fig
the way along th
way along the be
previous section
in a manner des

Comparison o
the sequence of
Figure 4 conveys
the first arrival
processing simila
about the sequer
that the time ser
process this time
sonogram appro
a priori knowled

an *a priori* sense: for any given application one can adjust the resolution so as to give the best view of the aspect of the behaviour one wants to bring out. Indeed it is often convenient to plot out pictures at a range of resolutions since, as has been seen in the sequence above, the changes in the pictures as the resolution changes are themselves interesting and informative.

2. APPLICATION TO THE BENDING BEAM

It has now been seen how sonograms perform, given data which is understood thoroughly in advance; one would not, of course, normally use any such complicated technique to study the behaviour of a stretched string. In this section the technique is applied to the next most simple system, an ideal bending beam. This has much of the simplicity of the string, and one still has a reasonable idea of what the results should be. However, it does introduce a new ingredient of great significance—dispersion. Waves on a beam with different frequencies travel at different speeds, and this immediately makes the problem less transparent.

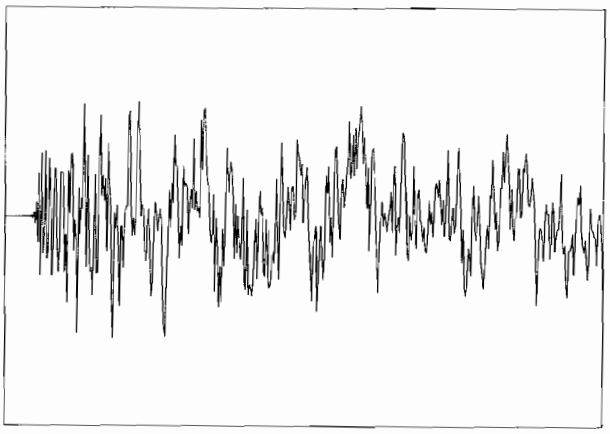

Figure 4. Time series for an ideal bending beam, impulse driven at 3/10 and observed at 4/5 of its total length.

This remark is illustrated by Figure 4, which shows the first portion of the time series analogous to Figure 1(b). This is the signal measured by an observer positioned 4/5 of the way along the beam following an impulse at time zero applied at a point 3/10 of the way along the beam: these are the same driving and observing points as were used in the previous section when investigating the string. The time series is a simulated one, calculated in a manner described in detail in the Appendix.

Comparison of Figures 1(b) and 4 reveals a striking difference: while in Figure 1(b) the sequence of events at the observing point is clear without carrying out any analysis, Figure 4 conveys no information to the naked eye apart from an initial time delay before the first arrival from the driving point reaches the observing point. Nevertheless, by processing similar to that carried out on the string data, one can obtain similar information about the sequence of events on the beam in time and frequency. Of course, if one knows that the time series corresponds to a beam with known dispersive behaviour, one could process this time series to yield a picture similar to Figure 1(b) [1]. The beauty of the sonogram approach, however, is that it yields much of the information without using any *a priori* knowledge about the system being studied.

First, one can calculate the power spectrum of the time series (using a much greater length of it than is shown in Figure 4). Figure 5 shows the result. Here the spectrum is plotted with a logarithmic vertical scale, with a total range of 30 dB in the box. One sees individual mode peaks as in the string case, but this time, instead of being equally spaced

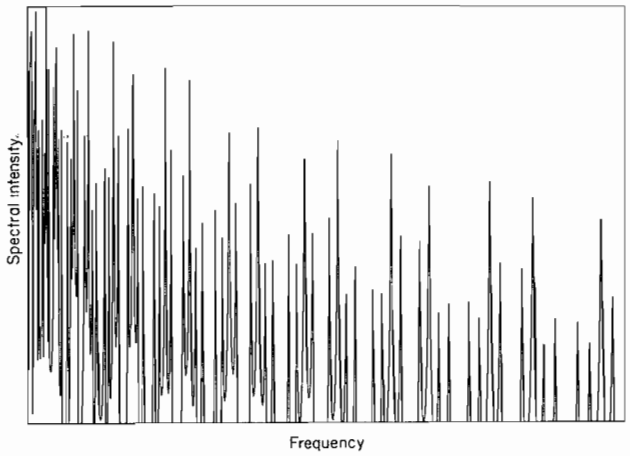

Figure 5. Power spectrum of the time series shown in Figure 4. Horizontal scale linear, vertical scale logarithmic with 30 dB range.

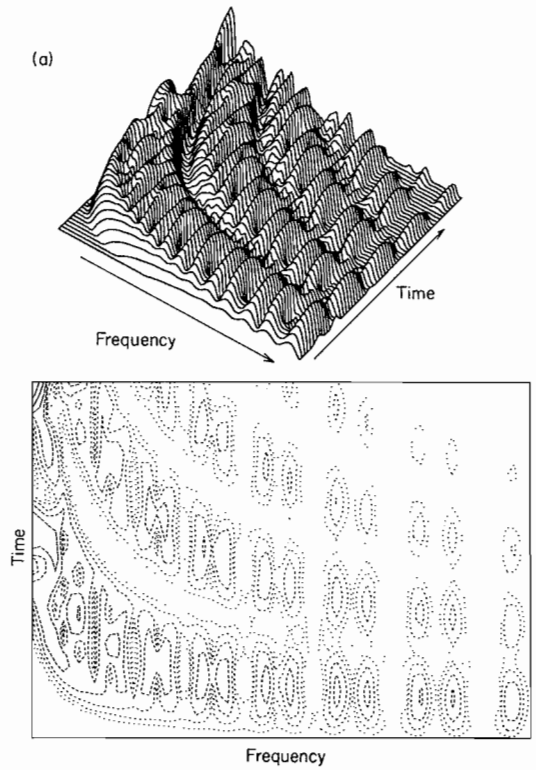

Figure 6. (a)-(c) Sonograms of the time series shown in Figure 4 with window lengths decreasing from (a)-(c) as given in the Appendix. Each sonogram is presented as a surface plot and as a contour map.

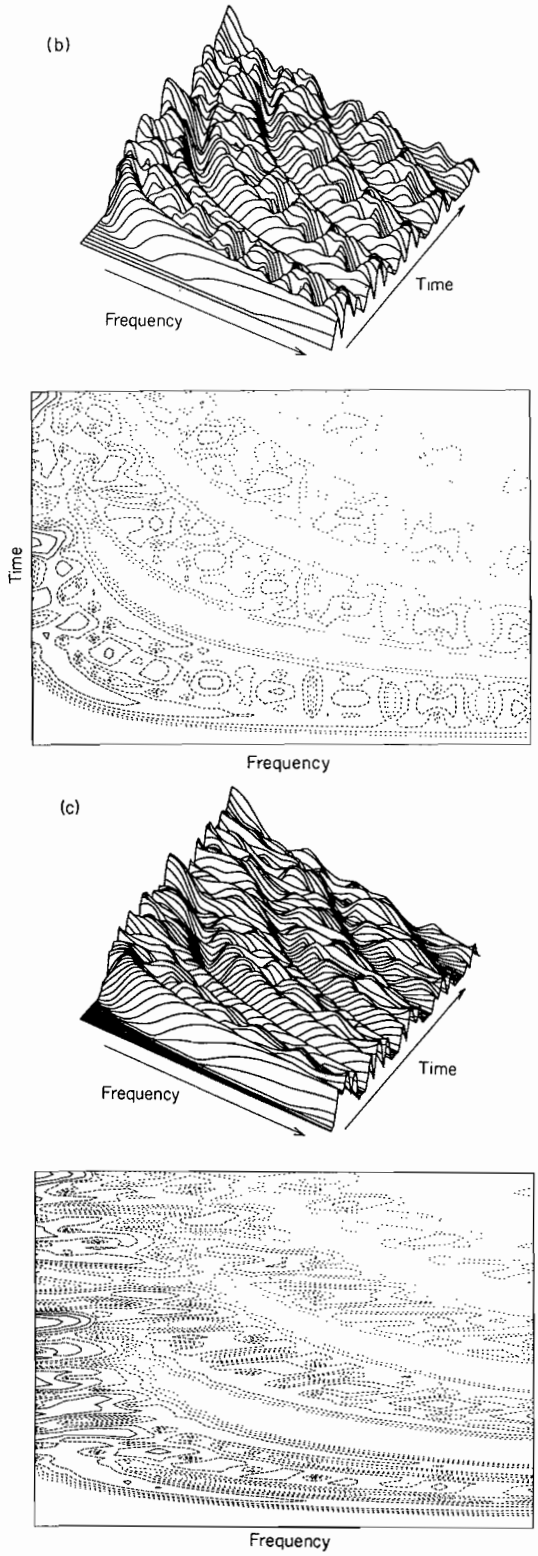

Figure 6—*continued.*

in frequency, the peaks crowd together towards zero frequency in accordance with the well-known behaviour of an ideal bending beam: the frequency of the nth mode is proportional to n^2. The modulation of peak heights as a result of the positions of driving and observing points is exactly as in the string case.

One can now calculate sonograms of the time series. Figures 6(a), (b) and (c) show three cases, with progressively decreasing window length. Again the details are given in the Appendix. In each case the total frequency range is the same as in the power spectrum (Figure 5) and the total time range is the same as that for which the time series was shown in Figure 4. Each sonogram is shown both as a surface plot and as a contour map: a surface plot is more readily interpreted without ambiguity, while a contour map is preferable for making measurements of the group velocity. As with the power spectrum of Figure 5, the surface plots have a logarithmic vertical scale with a "floor" imposed at 30 dB below the maximum height. This is done to show the behaviour more clearly: some damping was included in the simulation of the time series, and this together with effects of the dispersion of waves on the beam makes a linear scale less useful than in the string case. The contour maps have logarithmically spaced contours at 3 dB intervals, covering a total range of 24 dB. The highest contour is solid in each case, and the lower ones are plotted in progressively shorter dashes.

Before looking in detail at the sonograms, one should decide what one expects to see. If one were to restrict attention to a particular narrow frequency range, one would see the evolution in time and frequency of a wave packet composed of that range of frequencies. This will reflect back and forth along the beam at a speed equal to the group velocity of the beam at that frequency, exactly as was indicated in Figure 1(a) for the impulses on the string. Thus in that narrow frequency range, one should see four packets passing the observing point in each round-trip period of the beam at that group velocity. The only difference from the string will be that different frequency bands will produce different group velocities: the group velocity for a bending beam is zero at zero frequency, and increases proportional to the square root of frequency. Thus, one expects to see a sequence of behaviour in the sonograms generally similar to those for the string, except that the lines corresponding to a given arrival will no longer be straight, connoting synchronous arrival of all frequencies, but will be curved according to the inverse of the group velocity - frequency relation.

One is now ready to look in detail at the sonograms. Extreme cases of window length corresponding to Figures 3(a) and (d) have not been shown, but one can see a range of behaviour broadly mirroring that between Figures 3(b) and (c) but with arrival lines curved as described above. With the longest window, one still sees strong traces of the modulation pattern of peak heights in the power spectrum Figure 5, with only rather weak modulation in time showing the periodic nature of round-trip reflections of wave packets on the beam. In other words, each curving "stripe" contains a set of four passages of the packets past the observing point, not resolved at all in time because of the long window.

As the window length decreases, one begins to see more structure in time and less in frequency, as one expects. Since one is dealing with dispersing wave packets rather than ideal impulses here, one cannot achieve the ultimate time resolution represented by Figure 3(d). However, in Figure 6(c) one has reached a resolution similar to that of Figure 3(c), where the two outer arrivals of the wave packets are resolved quite clearly into ridges, but the middle two arrivals still overlap and therefore produce an interference pattern in frequency.

It is worthwhile pausing to look carefully at the contour maps of these latter two sonograms, since in the next section some sonograms will be shown at similar resolution

of measured da
the power of th
it is often bette
of which featur
technique of pr
However, some

Having seen
apply it to som
a range of non
exists a known
of different mo
variation of dis
the component
frequency, and
has to be an in
A theoretical m
[2], which is ap
with which one

The cylinder
radius and 28 1
thickness to rad
Warburton and
of course, the 1
about to be dis

To provide a
vibrational beh
was done by m
uniformly arou
with respect to
of positions tak
separated. This
measurements
and tapping at
Measurements
giving a spatial
were respectivel

Thus a set of
1, . . . , 8. These
described for th
group velocity
different values
of arrival as a fi
model. After th
discussed, to ex
of the sonogram

First, for one
are shown. Figu

of measured data, and one will want to be able to interpret these in some detail to show the power of the method for analyzing structural vibration in practice. Given the choice, it is often better to plot such contour maps in different colours to give a clear indication of which features are peaks and which valleys. That option is not available here, and the technique of progressively dotted lines goes some way toward conveying the same message. However, some practice is needed to interpret such plots in full detail.

3. APPLICATION TO A CYLINDRICAL SHELL

Having seen the sonogram technique working well on simulated data, one can now apply it to some real data. The cylindrical shell is chosen here as a structure which has a range of non-trivial behaviour which puts the method to the test, but for which there exists a known solution with which one can compare the results. A cylinder has a series of different modes of wave propagation, each associated with a different circumferential variation of displacement. In terms of cylindrical polar co-ordinates (r, θ, z) and time t, the components of displacement have the dependence $\cos n_c\theta \cos(kz - \omega t)$. Here ω is frequency, and k is the wavenumber along the cylinder axis. The variable n_c obviously has to be an integer, and the values 0, 1, 2, ... give the succession of waveguide modes. A theoretical model for the vibrations of cylinders has been given by Arnold and Warburton [2], which is appropriate to the frequency range of the measurements presented here and with which one can compare results.

The cylinder on which the measurements were taken was 11·3 m long, of 0·518 m mean radius and 28 mm thick. It happens that this geometry corresponds rather closely in thickness to radius ratio, the most important parameter, with Figure 2(d) of Arnold and Warburton and with the cylinder on which they have reported measurements. However, of course, the measurements which they have described are very different from those about to be discussed here and, in particular, do not involve sonograms.

To provide a direct comparison with the theory, it was first necessary to separate the vibrational behaviour of the cylinder corresponding to the different values of n_c. This was done by measuring response to an impulsive source at an array of sensors spaced uniformly around the circumference of the cylinder, and Fourier analyzing the results with respect to azimuthal angle θ. The response of the cylinder between a particular pair of positions takes the form $\sum a_{n_c}(t) \cos n_c\theta$, and by this process the functions $a_{n_c}(t)$ were separated. This process is here called "angular filtering". For practical convenience the measurements were made reciprocally, by using one accelerometer at a fixed position and tapping at points around the circumference by using a force transducer hammer. Measurements were made at 16 points, a convenient power of two for FFT purposes, giving a spatial Nyquist limit at $n_c = 8$. The positions of the driving and observing points were respectively at 3·61 m from one end, and 1·55 m from the other end.

Thus a set of nine angular-filtered time series was produced for the values $n_c = 0, 1, \ldots, 8$. These time series could then be analyzed by the sonogram technique exactly as described for the simulated data in the previous sections, to reveal the dependence of group velocity on frequency for each of the waveguide modes corresponding to the different values of n_c. First some results of that analysis are shown, compared with times of arrival as a function of frequency calculated according to the Arnold and Warburton model. After that, the results and some key features of cylinder vibration theory are discussed, to explain what is shown in the measurements and why they make a good test of the sonogram technique.

First, for one particular value of n_c, two sonograms with different time window lengths are shown. Figures 7(a) and (b) are both calculated from the data for $n_c = 3$, with window

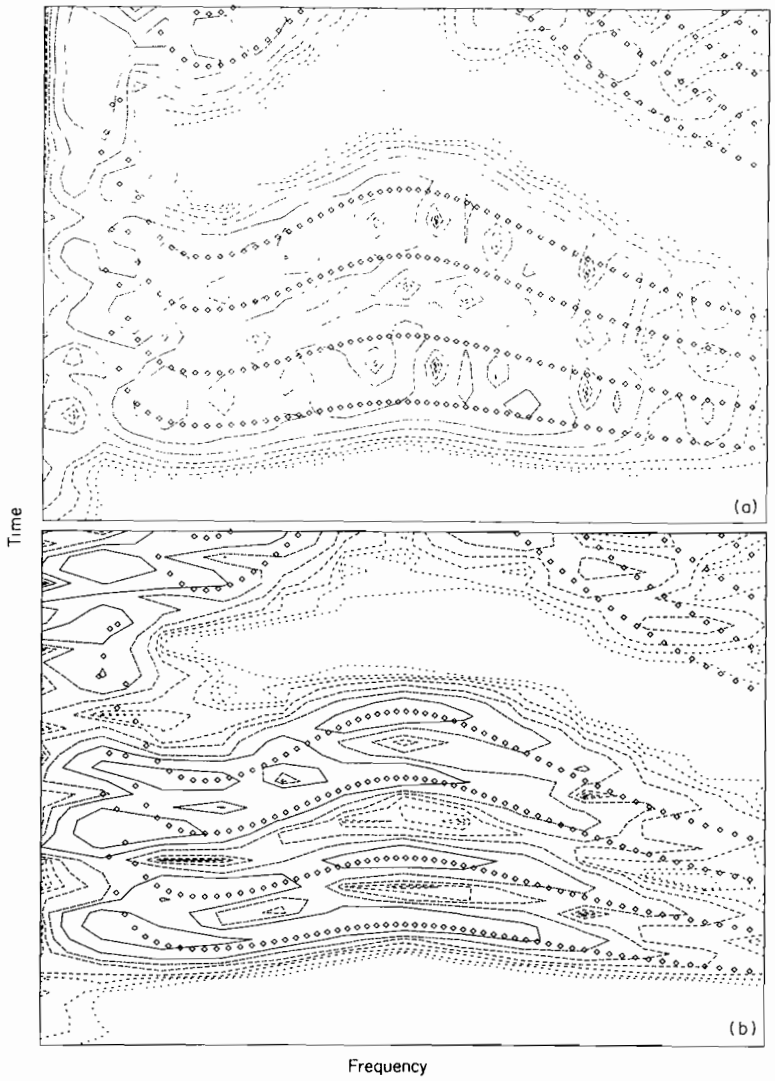

Figure 7. (a) and (b) Sonograms measured from a cylinder, for the waveguide mode with $n_c = 3$. The frequency scale is linear up to 2841 Hz, and the total time range is 30·89 ms. In (a) the window length is twice that used in (b) (see the Appendix). The plotted diamonds superposed show the times of arrival of wave packets predicted from the theory.

lengths differing by a factor of two (Figure 7(a) being the longer). Again, the details of the sonogram calculations are given in the Appendix. The contour maps show the measured sonograms, while the lines of plotted symbols superimposed on them show the times of arrival of the wave packets reflecting back and forth from the ends of the cylinder, calculated from the theory (but see the discussion of end corrections below). In both cases it can be seen that the level of agreement between theory and measurement is excellent. Recall that one is expecting each arrival to appear as a ridge, which may or may not be completely resolved. The eye should not be confused by the rising flanks of the response pattern: each line of plotted symbols should, and indeed does, lie along the top of such a ridge.

Comparing
much as one h
of four passag
group of four
there is some t
hand, all four
In calculatir
a rather *ad hoc*
the first arrival
theory, there i
predict the enc
was useful as a
Since there is n
of a pattern of
has been deduc
length came out
of the radius, w
Next the rang
8(a)–(c) were
respectively $n_c =$
arrival lines anc
length chosen h
amusing to see
more useful in p
first arrival lines
To understand
of the theory of
first few values o
and Warburton [
The frequency n
"breathing" reso
superimposed on
simply by calcula
apart of source a
There is a slight
For any given va
relation. These a
cylinder; radial, a
that is what has b
the radial branch
however, the radi
along the cylinder
evident. The arriv
of both curves cor
There are two q
since they are con
greater there is a
dependence cannc
bending ring with
common to all sucl

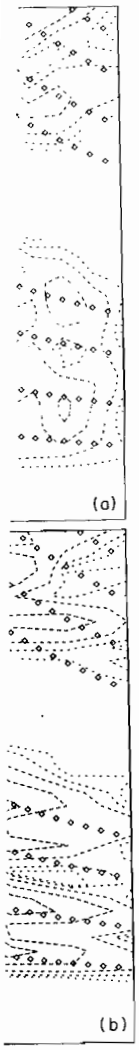

de with $n_c = 3$. The frequency
low length is twice that used
/al of wave packets predicted

). Again, the details of
iaps show the measured
:hem show the times of
: ends of the cylinder,
:ctions below). In both
ry and measurement is
a ridge, which may or
d by the rising flanks of
deed does, lie along the

Comparing the two figures, one sees the effect of changing the window length very much as one has now come to expect. In both cases, one sees clear signs of the first group of four passages past the observing point of the response to impulsive driving. The second group of four just shows at the top of the picture. In Figure 7(a), with the longer window, there is some temporal interference between the four arrivals. In Figure 7(b) on the other hand, all four are separately resolved but with the penalty of reduced frequency resolution.

In calculating the theoretical arrival times shown superimposed on these sonograms, a rather *ad hoc* assumption about end corrections for the cylinder had to be made. While the first arrival has been strictly predicted with no disposable parameters from the simple theory, there is no claim to have modelled a free-ended cylinder in sufficient detail to predict the end correction needed to give timings of reflected packets. Nevertheless it was useful as a guide to interpretation of the measurements to show the multiple reflections. Since there is no doubt about the qualitative interpretation of the measurements in terms of a pattern of multiple reflections (particularly Figure 7(b)), an end correction length has been deduced from the measurements and used to calculate the lines plotted. This length came out at 0·16 m (increasing the effective length of the cylinder), about one-third of the radius, which is entirely consistent with the qualitative expectations.

Next the range of behaviour associated with different values of n_c is illustrated. Figures 8(a)–(c) were all calculated with the same time window as Figure 7(a), and show respectively $n_c = 0$, 2 and 5. In all cases, one sees very good agreement with the theoretical arrival lines and the actual arrivals revealed by the measured sonograms. The window length chosen here seems to be the best compromise for the purpose. Although it is amusing to see the groups of four arrivals completely resolved as in Figure 7(b), it is more useful in practice to have the extra frequency resolution to show the shapes of the first arrival lines more accurately, particularly where these lines are rising or falling steeply.

To understand the features revealed by these figures, one needs to discuss some aspects of the theory of cylinder vibrations. The dispersion relations between k and ω for the first few values of n_c are shown in Figure 9, calculated according to the model of Arnold and Warburton [2] for a cylinder with the geometry of that used in these measurements. The frequency marked as f_r is the *ring frequency*, the frequency at which the radial "breathing" resonance of a ring of that radius occurs. The arrival lines which were superimposed on the measured sonograms were calculated from these dispersion curves simply by calculating the group velocity by differentiation, and dividing it into the distance apart of source and receivers in the measurement.

There is a slight complication with these dispersion curves which needs to be mentioned. For any given value of n_c, there are actually three separate branches of the dispersion relation. These arise from the three degrees of freedom of motion at a point of the cylinder; radial, axial and circumferential. Here only radial motion is of interest, since that is what has been measured. For values of n_c greater than zero, this means that only the radial branch has been plotted in Figure 9, with the other two ignored. For $n_c = 0$ however, the radial branch couples to the axial branch (that of compressional waves along the cylinder) so that we have plotted two branches. The coupling region is quite evident. The arrival times for the sonogram comparison were calculated from the parts of both curves corresponding to predominantly radial motion.

There are two qualitative features of these curves to which attention should be drawn since they are conspicuous features of the measurements. First, for values of n_c of 2 or greater there is a lower cut-off frequency below which waves with that circumferential dependence cannot propagate. This cut-off frequency is the resonant frequency of a bending ring with the given value of n_c, and is the usual waveguide cut-off phenomenon common to all such problems. At each cut-off frequency, the group velocity goes to zero.

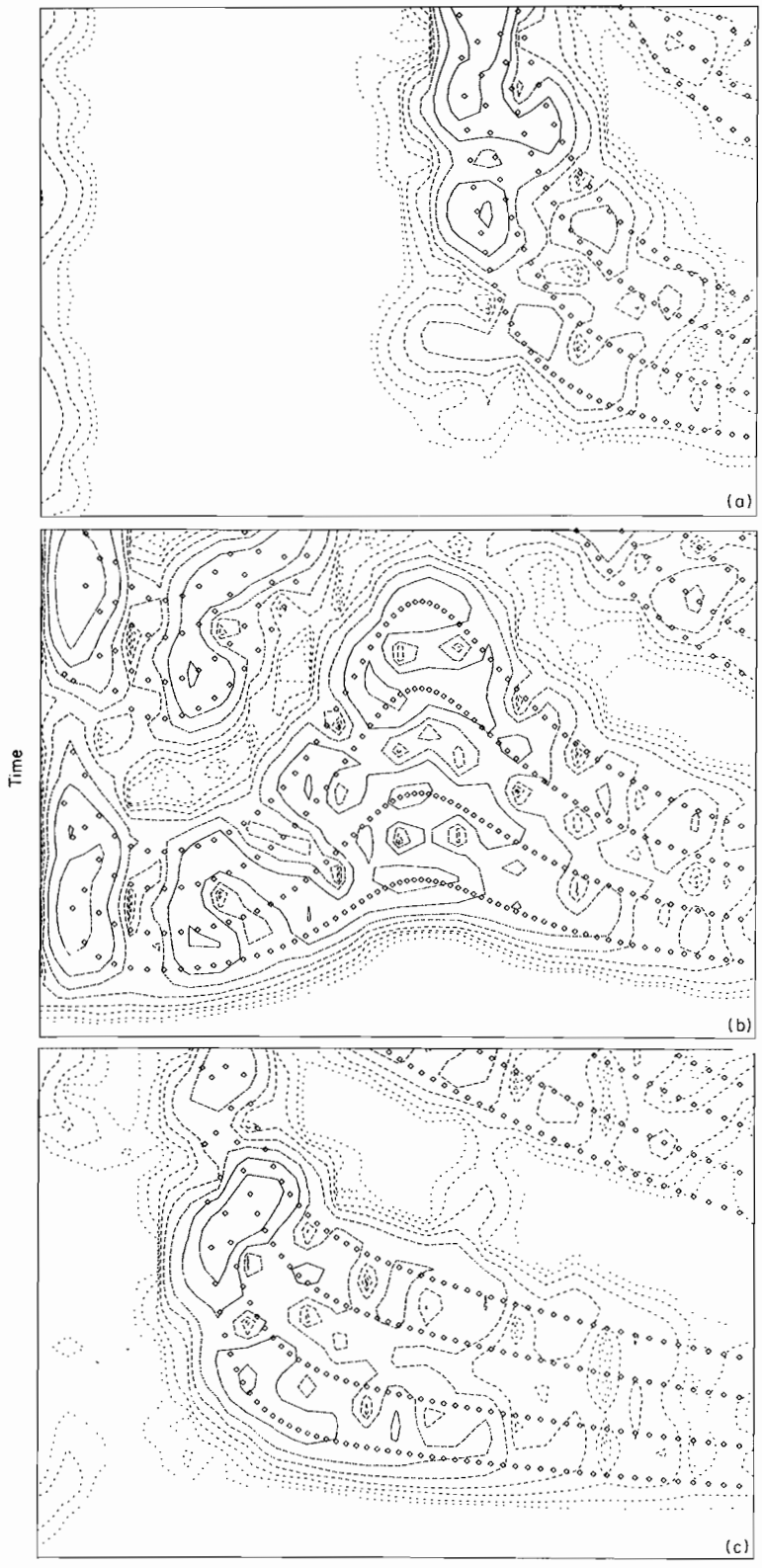

Figure 8. (a)–(c) Sonograms and predicted arrival times for waveguide modes $n_c = 0$, 2, 5 on the cylinder. The window length, frequency range and time range for the sonograms are the same as used in Figure 7(a).

Figure 9. Theoretically
wavenumber for the first f
7 and 8. The values of n_c
coupling of the compressi

Thus in the measure
the cut-off is approac
where the cut-off fre
pictures showing n_c =

The second feature
the physics of cylind
cylinder tends to vib
There is a circumferer
due to radial motion
from zero however, p
a large potential energ
very steeply for low
in-surface stretching r
circumferential comp
further, each curve is
the infinite flat plate

The effect of these
ring frequency. In ter
and this is very evid
strongly. It is still evi

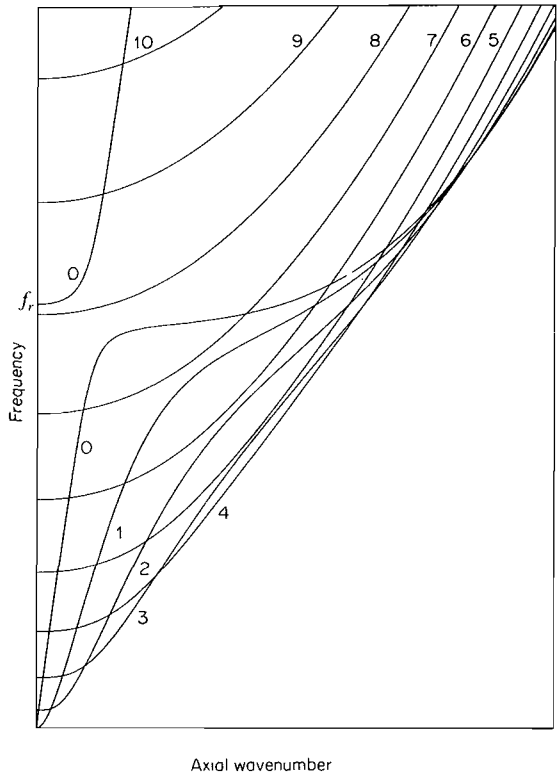

Figure 9. Theoretically predicted frequency dispersion curves for the cylinder, shown as a function of axial wavenumber for the first few values of n_c over the same frequency range as the sonograms presented in Figures 7 and 8. The values of n_c are marked on the curves. Note that the $n_c = 0$ curve is in two portions, because of coupling of the compressional and radial branches near the ring frequency.

Thus in the measurements one sees the first arrival line vanishing out of the picture as the cut-off is approached from above. This is particularly clear in Figure 8(c) for $n_c = 5$, where the cut-off frequency is highest. It can be seen going down towards zero on the pictures showing $n_c = 3$ (Figure 7) and 2 (Figure 8(b)).

The second feature relates to the shapes of the curves and requires a little delving into the physics of cylinder vibration. For values of the axial wavenumber k close to zero the cylinder tends to vibrate inextensionally; i.e., with little stretching of the shell surface. There is a circumferential component of the motion which compensates for any stretching due to radial motion exactly as for the low modes of a bending ring [3]. As k increases from zero however, particularly for low values of n_c, this circumferential motion implies a large potential energy due to in-surface shearing motion, so that the curves climb initially very steeply for low n_c. As the ring frequency is approached the energy penalty for in-surface stretching reduces, and the character of the motion tends to change so that the circumferential component is eliminated and the curves flatten out. As k increases still further, each curve is eventually dominated by axial bending energy and asymptotes to the infinite flat plate dispersion curve.

The effect of these three regimes is to make the low-n_c curves "hesitate" around the ring frequency. In terms of group velocity, a minimum occurs around the ring frequency, and this is very evident in the measurements. Figure 8(b), for $n_c = 2$, shows the effect strongly. It is still evident for $n_c = 3$ in Figure 7, but by $n_c = 5$ in Figure 8(c) it has more

)n the cylinder.
n Figure 7(a).

or less vanished since axial bending begins to be felt before the ring frequency relaxation can be reached. This rather subtle interplay between different physical effects is what makes the cylinder a good test structure to demonstrate the power of the sonogram technique, since the detailed shape of the arrival lines depends on the precise balance between these effects and thus on the substantial correctness of the theory.

The sonogram for $n_c = 0$ is somewhat different from the others. As explained above, two branches of the dispersion curve have been plotted for this value of n_c, but only the parts of both which correspond to predominantly radial motion are of interest here. The parts in question start at the ring frequency when $k = 0$, then pick up the other branch and eventually asymptote to the infinite plate-bending dispersion curve. This is brought out clearly in the measurement: one sees the arrival lines starting at the ring frequency, and getting faster as frequency increases. Another feature of Figure 8(a) to which attention should be drawn is the apparent signal near zero frequency. This is simply noise in the measurement: accelerometer signals have been integrated to give velocity plots, and background noise at low frequencies has thus been boosted so that it appears in the picture.

4. CONCLUSIONS

The principles of sonogram analysis of impulse responses of structures have been introduced. To introduce the technique without the complications of real data collection, it has first been demonstrated by using simulated data to examine the behaviour of two simple systems. In both cases it has been seen that a range of sonograms with varying lengths of data window can bridge the gap smoothly between direct inspection of the time series (a purely time-domain view) and conventional spectral analysis (a purely frequency-domain view).

The technique has then been used on real data for the various waveguide modes of a cylindrical shell. This somewhat complicated structure provided a non-trivial test of the method, and excellent agreement between the sonogram measurements and theory was demonstrated. Thus sonograms have been shown capable of giving a direct experimental determination of group velocity in a structure as a function of frequency. They have also proved capable, to an extent, of following multiple reflections within a finite system: both for the simulated bending beam data and for the measured data from the cylinder, the expected pattern of round-trip reflections was seen.

When applying this technique to impulse data from structures, whether simulated or real, the main problem lies in choosing the appropriate window length. The important thing to bear in mind is that there is not in any general sense a "best" window length. All sonograms, with whatever window length, contain more or less the same amount of information as the original time series or its Fourier transform. (Phase information is lost, of course, but could in principle be substantially recovered by Hilbert transform for causal signals such as one is dealing with here.) The choice of window length depends solely on what questions about the data one is trying to answer, and thus whether a bias more in favour of frequency resolution or more in favour of temporal resolution is wanted. In practice, it is usually best to do what has been done in each of the three sections in this paper: plot out sonograms with a range of window lengths. The changes in the pictures as the window length changes can be as revealing as any individual picture.

Finally it should be emphasized that it is not the sonogram technique itself for which any originality is being claimed here, but only the specific application to analysis of structural impulse responses. In studying the behaviour of such structures as regularly ribbed cylinders, it has been found that sonogram analysis along the lines described here is vital for detailed interpretation of measurements, and it is partly as a preliminary to

presenting that w
undoubtedly be
make.

This work has b
of Defence. The a
and much patien
Crighton and J. F

1. P. R. BRAZIER-S
75, 453–457. The
structures.
2. R. N. ARNOLD
Flexural vibratio
in A. KALNINS
Penn: Dowden, H
3. LORD RAYLEIG
re-issue. See arti

APPENDI

(a) THE STRING

The time series
samples. The pos
conveniently into
squared modulus
Fourier Transform
driving point). For
Hanning windowe
3(d), 8. The numb
the pictures cleare

(b) THE BEAM

The time series o
The nth mode sha
and the correspon
calculated by sum
that one cycle of
included, every m
again calculated b
following lengths
the number of line
each case.

(c) THE CYLINDER

The measuremer
figure being an art

presenting that work that this paper has been written. In any case, the technique could undoubtedly be of great benefit to many other people with structural measurements to make.

ACKNOWLEDGMENTS

This work has been carried out with the support of the Procurement Executive, Ministry of Defence. The authors are particularly grateful to Dr I. Roebuck for helpful discussions and much patience during this programme of work. We also thank Professors D. G. Crighton and J. E. Ffowcs Williams for useful comments.

REFERENCES

1. P. R. BRAZIER-SMITH, D. BUTLER and J. R. HALSTEAD 1981 *Journal of Sound and Vibration* **75**, 453–457. The determination of propagation pathlengths of dispersive flexural waves through structures.
2. R. N. ARNOLD and G. B. WARBURTON 1949 *Proceedings of the Royal Society* **A197**, 238–256. Flexural vibration of the walls of thin cylindrical shells having freely supported ends. (Reprinted in A. KALNINS and C. L. DYM 1976 *Benchmark Papers in Acoustics*, Volume 8, Stroudsberg, Penn: Dowden, Hutchinson and Ross.)
3. LORD RAYLEIGH 1877 *The Theory of Sound*, Volume 1. New York: Dover, second edition, 1945 re-issue. See articles 192a, 234 and 235.

APPENDIX: THE CALCULATION OF THE DATA AND SONOGRAMS

(a) THE STRING

The time series of Figure 1(b) was calculated in discrete form with a period of 80 samples. The positions of driving and observing points as given in the text divide conveniently into this figure, so they are exact. The power spectrum of Figure 2 is the squared modulus over the full range up to the Nyquist frequency of a 2048-point Fast Fourier Transform (FFT), starting at time zero (when the impulse was delivered at the driving point). For the sonograms of Figure 3 time windows of the following lengths (all Hanning windowed) were used: Figure 3(a), 256; Figure 3(b), 64; Figure 3(c), 32; Figure 3(d), 8. The number of lines drawn in the hidden-line surface plots was chosen to make the pictures clearest, and for that reason is not the same in all pictures.

(b) THE BEAM

The time series of Figure 4 was calculated from a sum over normal mode contributions. The nth mode shape for a beam of length a with simply supported ends is $\sin(n\pi x/a)$, and the corresponding frequency is proportional to n^2. The discrete time series was calculated by summing the contributions from the first 100 modes, with a timescale such that one cycle of the fundamental would occupy 20 000 samples. Damping was also included, every mode having a Q factor of 500. The power spectrum of Figure 5 was again calculated by 2048-point FFT. For the sonograms of Figure 6 time windows of the following lengths were used: Figure 6(a), 128; Figure 6(b), 64; Figure 6(c), 32. Again, the number of lines plotted in the hidden-line plots was chosen for maximum clarity in each case.

(c) THE CYLINDER MEASUREMENTS

The measurements on the cylinder were digitized at a rate of 15151 Hz (the curious figure being an artefact of our logging system). All sonograms show 40 spectra, over a

frequency range 0–2841 Hz and a total time range of 30·89 ms. This was achieved by stepping the window forward by 12 points between each pair of spectra. For Figures 7(a) and 8 an FFT length of 128 was used, the first 25 frequency points (including DC) being shown in the plots. For Figure 7(b), an FFT length of 64 was used and 13 points were plotted.